JOURNAL OF GEOPHYSICAL RESEARCH, VOL. 106, NO. A1, PAGES 23-31, JANUARY 1, 2001

The profile of the hydrogen H_β emission line in proton aurora

D. Lummerzheim
Geophysical Institute, University of Alaska, Fairbanks, Alaska

M. Galand[1]
Space Environment Center, NOAA, Boulder, Colorado

Abstract. Models of hydrogen-proton transport in proton aurora predict the line profile of the hydrogen emissions from specified incident proton precipitation. We are using a model that includes collisional angular redistribution which leads to upward moving proton and hydrogen fluxes. For ground-based observation in the magnetic zenith this causes a small Doppler broadening toward the red in the line profile. The precipitating energetic hydrogen atoms are responsible for the prominent Doppler shift toward the blue. The resulting line profile has thus both a widened red and a widened blue wing. Using a spectrometer with sufficient spectral resolution to distinguish the red-shifted wing of the line from the instrumental line broadening, we obtain H_β line profiles (486.1 nm). Comparing the predicted line shapes to our observations, we find the red-shifted wing is due to upward moving hydrogen as predicted by the angular redistribution in the model calculations. The shape of the blue-shifted wing, rather than the location of the peak of the blue-shifted line profile, is a suitable indicator of the mean energy of the precipitating proton flux.

1. Introduction

When energetic protons precipitate into the thermosphere they undergo collisions with the ambient atmospheric gas. In charge-exchange collisions a proton turns into an energetic hydrogen atom, which in turn can get stripped of its electron in a subsequent collision. Eventually, the proton flux will turn into a mixture of energetic protons and hydrogen atoms. Protons are bound to spiral along the magnetic field direction; hydrogen can cross field lines. Unlike the narrow and well-defined curtains of electron aurora, the proton aurora is thus spread out into a diffuse glow. Elastic and inelastic collisions can cause small deflections of the velocity. This causes pitch angle changes in the proton flux and results in a small backscattered component that escapes upward. The energetic particles loose energy in collisions with ambient neutrals. Part of that energy is transfered to secondary electrons (proto-electrons), which then also contribute to the auroral emissions. To simulate such a proton aurora, one must solve a combined proton-hydrogen-electron transport equation. Several approaches are possible for such a model, ranging from quasi-analytical approaches [*Jasperse and Basu*, 1982; *Basu et al.*, 1987], Monte Carlo simulations [*Kozelov*, 1993; *Decker et al.*, 1996; *Lorentzen et al.*, 1998; *Synnes et al.*, 1998; *Gerard et al.*, 2000], to explicit solutions of the coupled Boltzmann equations [*Basu et al.*, 1993; *Strickland et al.*, 1993; *Galand et al.*, 1997, 1998].

Hydrogen emissions originate exclusively from proton aurora. Neither the secondary electrons nor the precipitating electrons in electron aurora contribute to the hydrogen emissions, since the density of ambient hydrogen in the thermosphere at the altitude of aurora is negligible. In this study we focus on a typical signature of the proton precipitation, the line profile of the H_β emission, and we adopt results from the proton-hydrogen transport code from *Galand et al.* [1997]. The proton-hydrogen transport equations allow for charge exchange, stripping, ionization, excitation, and elastic collisions. The model is one-dimensional in space (along the magnetic field direction) and time independent. The effect of horizontal spreading can be taken into account by assuming a spreading factor [*Jasperse and Basu*, 1982]. This affects the predicted brightness, but has no effect on the shape of the line profile, when the model is applied to the center region of a precipitation event.

[1]now at: Center for Space Physics, Boston University, Boston, MA 02215

Paper number 2000JA002014.
0148-0227/01/2000JA002014$09.00

In this paper we present ground-based observations of line profiles of the H_β emission. From several months of observations during the 1998 and 1999 winter seasons in Poker Flat, Alaska, we discuss the data from one night by way of example. Our main focus is to use the observations to illustrate and confirm features of the Doppler line profile of the H_β emission that are predicted by model calculations.

2. Predictions of the Proton Aurora Model

The solution of the coupled proton-hydrogen transport equations is described in detail by *Galand et al.* [1997, 1998]. We use that model to study the systematic behavior of the hydrogen emission Doppler profiles. Given an incident proton flux at the top of the atmosphere, the particle fluxes are determined from the solution of the steady state Boltzmann equations as a function of altitude, energy, and pitch angle. The model describes the energy loss through collisions by dissipative forces, and angular redistribution of collisional and magnetic origin are included [*Galand et al.*, 1997]. This proton transport code has been successfully validated by comparison with rocket particle data [*Søraas et al.*, 1974] and by comparison with the model of *Basu et al.* [1993] [*Galand et al.*, 1997]. From the particle fluxes and excitation cross sections we calculate the hydrogen emission Doppler profile [*Galand et al.*, 1998].

The incident flux at the top of the atmosphere is assumed to be purely protons and isotropic over the downward hemisphere [*Søraas et al.*, 1974; *Basu et al.*, 1987]. The characteristic energy of the Maxwellian, E_0, half of the mean energy, is varied between 1 and 20 keV, typical for nightside auroral proton precipitation [*Hardy et al.*, 1989]. Since the transport equations are linear with respect to the incident energy flux, the energy flux has no effect on the shape of the Doppler profile. The neutral atmosphere is specified by the Mass Spectrometer and Incoherent Scatter model (MSIS-90) [*Hedin*, 1991], for the location of Poker Flat (66.56° N, 148° W) at 0230 local time in winter, with a magnetic activity index *Ap* of 50 and a solar index $F_{10.7}$ of 150. The model assumes a vertical magnetic field. The collision cross-section set and collision energy losses are discussed by *Galand et al.* [1997, 1998]. The incident beam is assumed sufficiently broad (larger than 250 km) that beam spreading associated with the horizontal diffusion of the hydrogen atoms can be neglected [*Jasperse and Basu*, 1982].

The Doppler profiles in proton aurora depend not only on the energy distribution of the energetic hydrogen but also on the observing geometry. The velocity vector of a gyrating proton is preserved in the linear velocity of a hydrogen at the moment of a charge-exchange collision. For observations perpendicular to the geomagnetic field the perpendicular velocity component of the gyration of the protons and the phase angle of the gyration define the line of sight velocity of the hydrogen that leads to the Doppler shift of a subsequent emission. The uniform distribution of the phase angle results in a symmetric Doppler profile centered on the unshifted emission wavelength. For observations along the magnetic field the line of sight velocity of the hydrogen is determined by the parallel velocity of the gyrating protons, while the phase angle does not contribute. This leads to asymmetric Doppler profiles, where the blue and red wings represent the velocity distribution of down and upward moving hydrogen.

Figure 1 shows examples of the H_β line profile for observations along the magnetic field for characteristic energies of 1, 3, 10, and 20 keV. Each profile is normalized for this comparison. The relative normalization is equivalent to increasing the energy flux as E_0 increases, giving $\sim$ 1, 2.5, 7, and 13.5 $\mathrm{mW\,m^{-2}}$, for the four characteristic energies, respectively. The dashed lines show the calculated emission Doppler profiles. For comparison with observations we have convolved these line profiles with a triangular instrument function with a full width at half maximum (FWHM) of 0.43 nm. The horizontal bar at the bottom indicates the simulated instrument resolution. The solid lines show the Doppler line profile after convolution with the instrument function. These model runs were made without

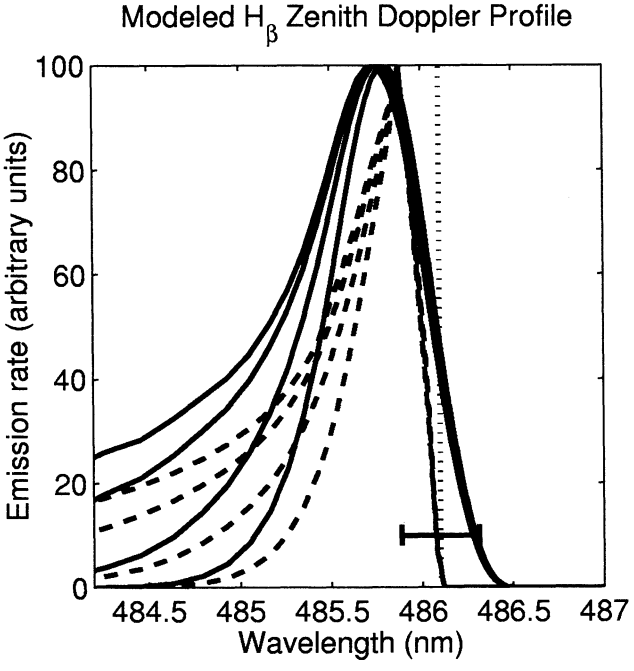

Figure 1. H_β line profiles from model calculations without angular redistribution for incident Maxwellian proton spectra with E_0 of 1, 3, 10, and 20 keV. The dashed lines are the emission Doppler profiles; the solid lines are the same profiles convolved with an instrument function with full width at half maximum (FWHM) of 0.43 nm. The dotted vertical line indicates the unshifted emission wavelength (486.1 nm); the horizontal bar shows the instrument FWHM. Each profile is normalized for comparison. The blue wing of the line profile brightens as E_0 increases.

including angular redistribution. The peak of the profile shifts very little with increasing characteristic energy, while the blue wing of the profile shows a dramatic relative increase with increasing E_0. The emission at the peak of the profile originates from hydrogen in the lower thermosphere that has undergone significant energy degradation owing to collisions, while the original high-energy precipitation is responsible for the extreme blue-shifted wing of the profile. As E_0 increases, the number of high-energy hydrogen also increases, causing the lifting of the extreme blue wing. The low-energy hydrogen arises from energy degradation in the transport process and is fairly independent of the initial energy distribution of the precipitating protons.

Galand and Richmond [1999] have shown that angular redistribution from magnetic mirroring in an incident proton beam has no significant effect on the hydrogen emission profile. Mirroring is important only at high altitudes, while the emissions are dominated by the low-altitude fluxes. On the other hand, collisional angular redistribution is included as it is efficient in the region where the hydrogen emissions originate [*Galand et al.*, 1998]. It is applied to N_2 and O_2 for energies below 1 keV, assuming the same elastic cross sections for both species. A forward scattering approximation is assumed for atomic oxygen. The phase functions and the N_2 elastic cross sections are described by *Galand et al.* [1998]. The phase function is based on the Rutherford formula with a screening parameter set to 0.001. Galand et al. point out the importance of angular redistribution in elastic and inelastic collisions. *Gerard et al.* [2000] reiterates this statement and adds that use of the proper phase function is also important to obtain the correct shape of the Doppler line profile. Gerard et al. compare their Monte Carlo simulation results, which use stochastic scattering angles as Galand et al. do, to previous Monte Carlo simulations by *Kozelov* [1993] who uses an average scattering angle approximation. Both, Galand et al. and Gerard et al. find that the use of the proper phase function has a significant impact on the shape of the Doppler line profile.

The effect of angular redistribution in elastic scattering and charge-exchange collisions on the Doppler profile of the H_β line is shown in Figure 2. The Doppler profile is widened by the inclusion of scattering processes. Scattering has thus a similar effect as an increase in energy. However, the widening due to scattering is symmetric, while an increase in energy only affects the blue wing of the profile (Figure 1). A widening of the red-shifted wing of the line profile beyond that of the unshifted line would thus be observational evidence of collisional angular redistribution. These model predictions motivated an observational program to detect the red-shifted wing of the Doppler line profile.

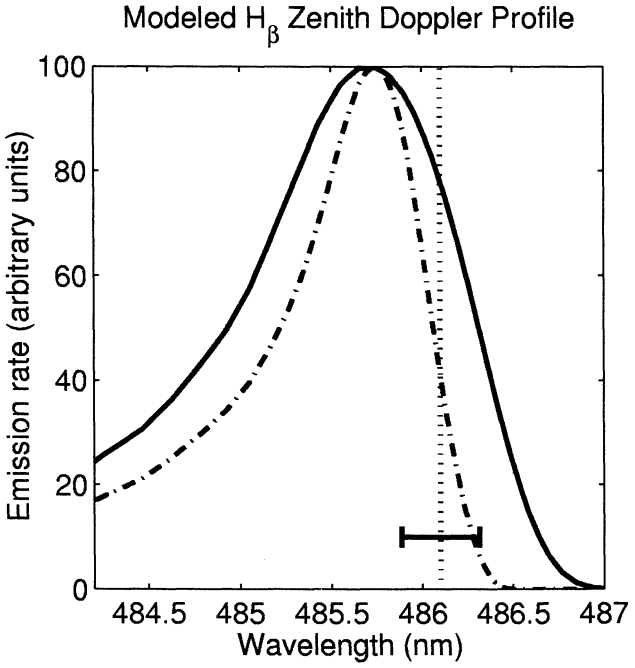

Figure 2. Normalized H_β line profiles for incident protons with $E_0 = 10$ keV without (dash-dotted line) and with (solid line) collisional angular redistribution. Both line profiles are convolved with the instrument function (FWHM of 0.43 nm). The scattering results in upward flowing hydrogen causing an increase of the relative brightness of the red wing over the nonscattering case.

3. Observations of Hydrogen Emission in Proton Aurora

3.1. Instrumental Setup and Calibration

For our observations we select the H_β line at 486.1 nm, since it is fairly isolated from other auroral and airglow emission features. N_2 Vegard-Kaplan emissions from electron aurora in this wavelength region are weak and contribute to a raised background brightness in the vicinity of the H_β line. Even though the H_α line at 656.3 nm is brighter, the close spectral proximity to the bright N_2 first positive emission makes it difficult to obtain clean line profiles. For the observations we used a 1-m Ebert-Fastie spectrometer at Poker Flat. The grating of the spectrometer is driven by a computer-controlled stepper motor, scanning a range from 478 to 487 nm every 16 s. We selected a slit width of 1 mm. The instrument was originally built by William G. Fastie [*Fastie*, 1952] and was consequently improved by *Sigernes et al.* [1996]. The field of view is 7° around the magnetic zenith. For wavelength calibration we took spectra from a hydrogen and xenon lamp before and after the sky observations. We found excellent repeatability for the mapping from stepper motor steps to wavelength: calibration spectra from the beginning of a night overlap with those from the end of a night. However, the stepper motor and gearbox driving the grating exhibited a small nonlinearity in the step count to wavelength conversion. The xenon lamp has three discrete lines

(480.7, 483.0, and 484.3 nm) in the 9-nm window of our wavelength scan, and the proper conversion from grating angle to wavelength [*Dick et al.*, 1970; *Sigernes et al.*, 1996] does not allow to fit all three Xe and the H_β line simultaneously. This indicates a nonlinearity in the conversion from stepper motor steps to grating angle which amounts to about ± 0.2 nm in the center of the 9-nm scan, comparable to half the spectral resolution. This nonlinearity is consistent from scan to scan and remained constant over several months of observations. It is most likely attributable to the gearbox that connects the stepper motor to the grating.

The line widths of the Xe and H lines serve to verify the spectral resolution of the instrument. Using the fitting procedure outlined below, we found the FWHM to be 0.43 nm. It should be stressed that the relative position of each line from the calibration lamps remained constant over time. The line profile of the stationary hydrogen calibration lamp gives a very precise reference wavelength for the H_β emission. In our analysis we have used the H_β line and the xenon line at 480.7 nm to calibrate the instrument scans in wavelength.

We operated the spectrometer during moon-down periods in March 1998 and spring and fall 1999. In this study we present data from a bright night, March, 21, 1998. A colocated calibrated meridian scanning photometer (MSP) indicated H_β brightness up to 100 R during our observations. An auroral breakup started at $\sim$ 0830 UT, leading to bright aurora over most of the sky until 1130 UT. Figure 3 shows a spectrogram of the H_β line during most of this interval. Usable line profiles can be obtained by co-adding individual wavelength scans. The spectra in Figure 3 are generated by averaging five scans, giving a time resolution of 80 s.

3.2. Analysis of the Observed Line Profiles

We have analyzed the data by fitting synthetic line profiles to averaged scans, using a nonlinear least squares fitting method [*Press et al.*, 1989]. Since the Doppler shift from the energy and pitch angle distribution of the precipitating particles causes an asymmetrical H_β line profile, we have constructed a synthetic line profile $I(\lambda)$ from a Gaussian shape with different half widths on the blue and red sides of the peak. To account for contamination by electron aurora, our fit also includes a wavelength-independent background:

$$I(\lambda) = I_L \exp\left[-\left(\frac{\lambda - \lambda_0}{\Delta(\lambda)}\right)^2\right] + I_B. \qquad (1)$$

I_L and I_B are the intensity of the line above the background and the background level, λ_0 is the wavelength of the peak of the line, and $\Delta(\lambda)$ is the wavelength-dependent half width:

$$\Delta(\lambda) = \frac{1}{2}\frac{1}{\sqrt{\ln 2}}\left[1 - \tanh\left(\frac{\lambda - \lambda_0}{\lambda_s}\right)\right](\lambda_b - \lambda_r) + \lambda_r. \qquad (2)$$

λ_b and λ_r are the half widths on the blue and red side of the line profile; the hyperbolic tangent (tanh) function is used as an analytic representation for a step function. The parameter λ_s defines the steepness of the step. The parameters λ_0, λ_b, λ_r, I_L, and I_B are obtained by a nonlinear least squares fit of the function $I(\lambda)$ to the data. Figure 4 illustrates the fitting parameters.

We can apply this fitting procedure to spectra from the hydrogen calibration lamp. In that case we find

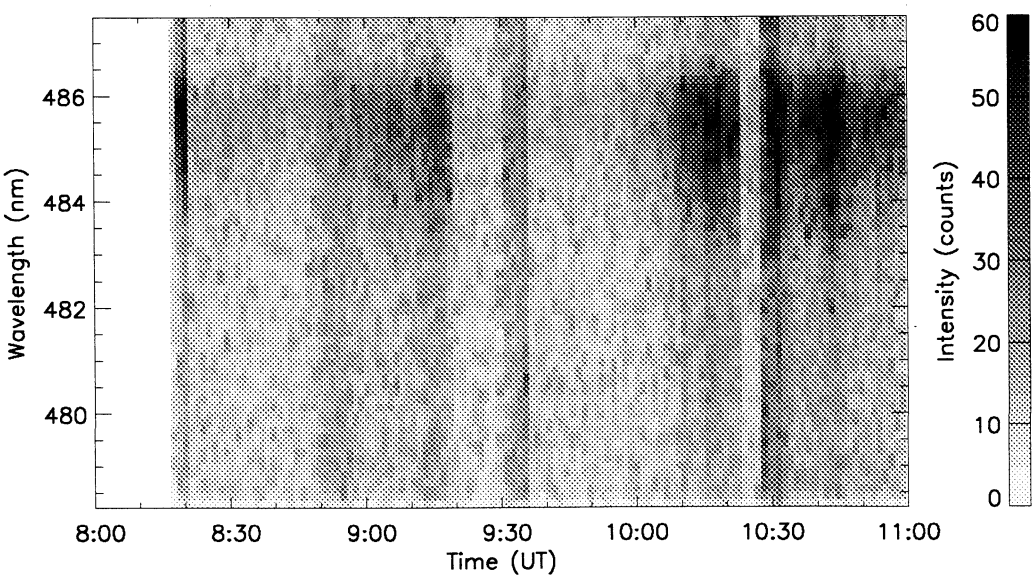

Figure 3. Spectrograms of H_β for March 21, 1998, obtained by averaging five scans for a time resolution of 80 s. Brightness is in uncalibrated counts. A co-located meridian scanning photometer (MSP) indicated H_β of up to 100 R at $\sim$ 1045 UT.

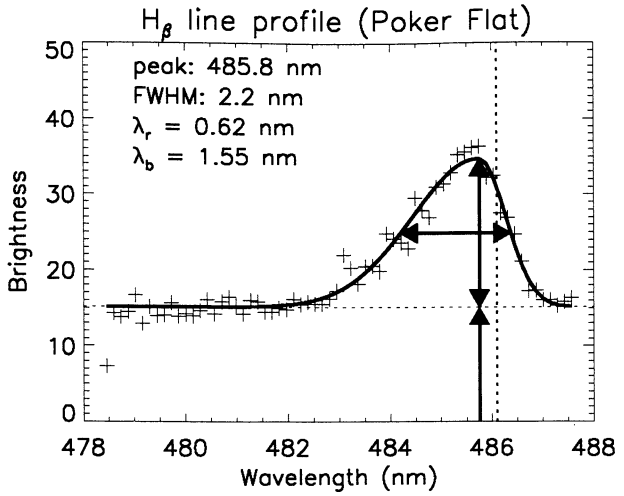

Figure 4. Example of a fitted spectral shape from February 12, 1999, at 1203 UT. The crosses are sky observations from spectrometer; the solid line shows the resulting fitted line profile. The individual parameters of the synthetic line shape are indicated by arrows: background level, line brightness above the background, and half widths of the short- and long-wavelength wings. The vertical dotted line shows the unshifted H_β wavelength.

that the line profiles are not exactly symmetric, indicating a slight misalignment of the optical elements in the spectrometer. We averaged 80 scans of observing a hydrogen lamp and found the short- and long-wavelength half widths to be $\lambda_b = 0.23$ and $\lambda_r = 0.20$ nm, giving a FWHM of 0.43 nm. This asymmetry tends to make the short-wavelength wing of the lines slightly wider than the long-wavelength wing, but this asymmetry is too small to affect our conclusions.

3.3. Interpretation of the Blue-Shifted Wing of the Line Profiles

For auroral spectra this fitting procedure gives the brightness of the hydrogen emission, the brightness of the background, which is attributed to electron aurora, the wavelength of the peak of the Doppler-shifted H_β line, and the width of the blue-shifted and red-shifted wings of the line. Figure 5 shows a 20-min section of the data from March 21, 1998, where a steady increase in H_β brightness occurred. We have averaged 15 scans (4 min) to improve the signal-to-noise ratio, and have we removed the wavelength-independent background brightness from the data. Three examples of data and fitted line shape are shown below the spectrogram. Because we do not have independent measurements of the precipitating proton fluxes, we cannot confirm the variation of the line width and blue shift with the proton mean energy. However, it is likely that the mean energy of the protons increases as the proton aurora brightens. The line width increased from 1.77 to 2.57 nm during the 15 min of this observation. The same increase can be seen by comparing the spectral brightness of the blue-shifted wing at 484 nm to that of the peak. This ratio changes from 0.22 to 0.52. We show this ratio since it is easier to measure than the line width and indicates the possibility of using two narrow interference filters, separated by ~ 2 nm, to obtain a measure of the mean energy of the proton precipitation. The data show only a small variation in the wavelength of the peak of the line, and the data exhibit more variability in the half width and the relative brightness of the blue wing of the line profile. This is in agreement with the model predictions from Maxwellian precipitating proton spectra. The model results from *Galand et al.* [1997, 1998] are shown in Figures 1 and 2 and clearly demonstrate the change of the shape of the line profile. *Gerard et al.* [2000] studied the Lyman-α Doppler line profile using Monte Carlo simulations, and they also conclude that the entire line profile must be considered to infer the energy of the incident proton flux. The model of Gerard et al. even predicts that the peak of the Lyman-α reduces its Doppler shift as the mean energy of incident proton Maxwellian distributions increases. If we assume that the increase of the line width in our data can be interpreted as an increase of the mean energy of the precipitating protons, we cannot confirm this prediction. The change of the peak wavelength for Lyman-α that Gerard et al. predict is, however, small (changing from 0.1 to 0.07 to 0.045 nm for mean energies of 1, 8, and 40 keV, respectively), and this change is likely not detected with the resolution of our instrument.

From observations of dayside proton aurora, *Deehr et al.* [1998] see a more pronounced variation in the wavelength of the peak of the Doppler-shifted line. They interpret this fact as an indication that the dayside proton aurora is dominated by mono-energetic or narrow Gaussian energy spectra of the precipitating protons. Modeling of mono-energetic proton precipitation by *Lorentzen et al.* [1998] and *Gerard et al.* [2000] supports this hypothesis. *Lorentzen et al.* [1998] and Deehr et al. argue that dayside proton precipitation is likely to be mono-energetic owing to the "velocity filter" resulting from dayside reconnection and convection. Nightside proton precipitation is expected to have broader energy distributions [*Hardy et al.*, 1989].

During bright proton aurora (100 R of H_β), we can get meaningful fitted line shapes at much higher time resolution. Figure 6 shows the brightest period of that night with only two scans averaged, giving a time resolution of 32 s. Comparing the half width and brightness ratio at 484 nm to peak brightness with the earlier period shown in Figure 5, we see the same systematic behavior. The FWHM has increased to 2.63 nm at the brightest spot, and the brightness ratio has increased to 0.65. Even though a slight shift of the wavelength of the peak to larger Doppler shifts for broader line width (i.e., opposite to the direction predicted by *Gerard et al.* [2000] for Maxwellian proton distribution) may be seen in the spectrogram, the variation of the brightness

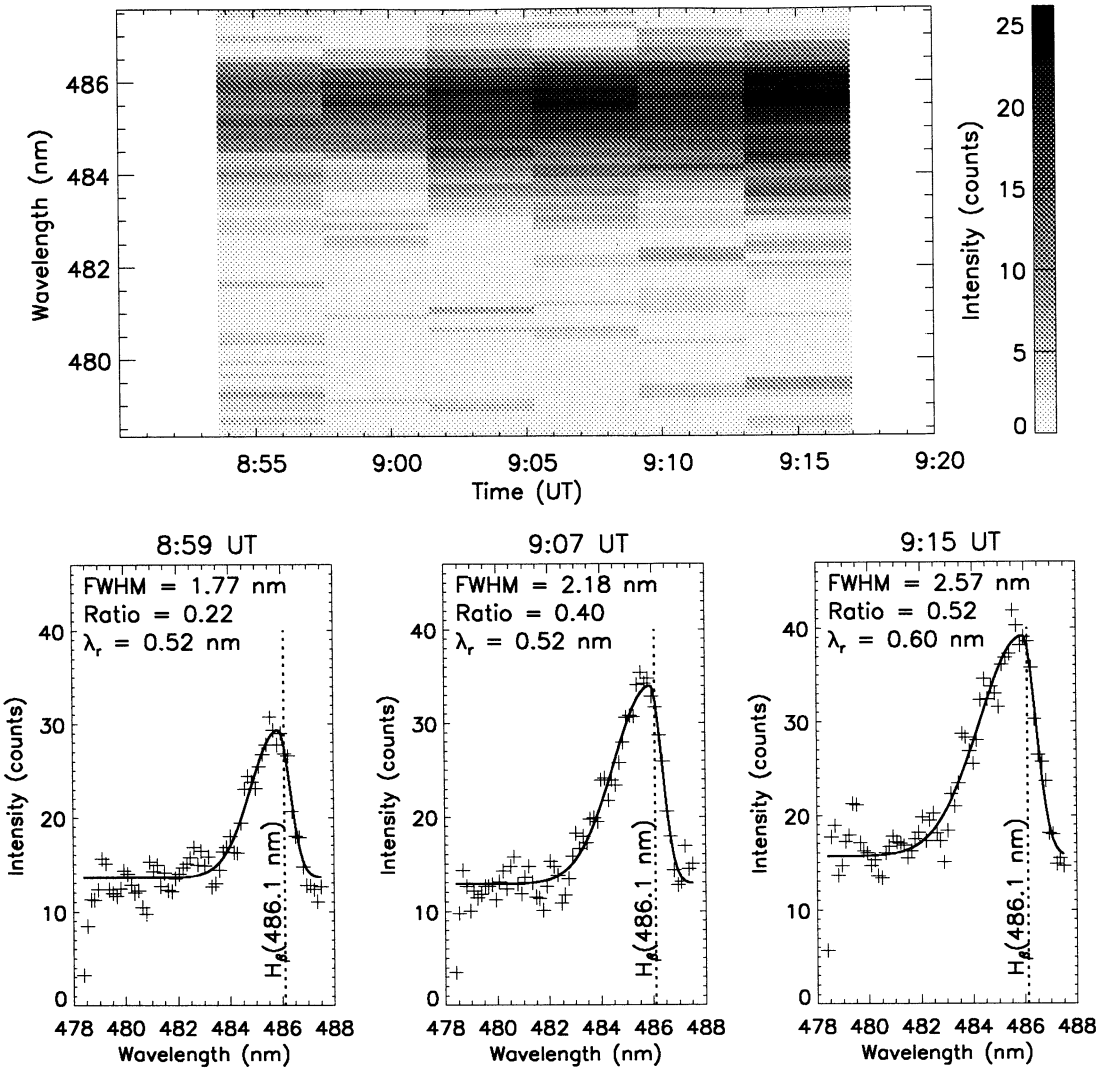

Figure 5. (top): Spectrograms of H_β for March 21, 1999, obtained by averaging 15 scans for a time resolution of 4 min. We have subtracted the fitted background. (bottom): Three line profiles from this period. Crosses indicate the observed line profile; the solid line is the fit. The unshifted H_β wavelength is shown by the vertical dotted line. The FWHM, the half width of the red wing λ_r, and the brightness ratio at 484 nm to the peak brightness are given in each panel. Note the increase of FWHM and the ratio as the brightness increases.

ratio is much more dramatic. Model calculations show that this behavior must be interpreted as an increasing proton energy.

3.4. Interpretation of the Red-Shifted Wing of the Line Profiles

Previous observations [*Eather*, 1966; *Sigernes*, 1996] showed a significant red wing of the line profile. *Eather* [1966] considered the effect of magnetic mirroring but concluded that the red-shifted wing in his observations was due to the instrument's spectral resolution of 0.8 nm. Magnetic field effects on the line profile have been discussed by *Galand and Richmond* [1999], who found no significant effect on the red shift. *Sigernes* [1996] and *Lorentzen et al.* [1998] operated the same 1-m Ebert-Fastie spectrometer with a wider slit giving

Table 1. Observed Half Width of the Red Wing

Date	Time, UT	λ_r, nm
calibration lamp		0.20
Feb. 12, 1999	1203	0.62
Mar. 21, 1998	0856	0.45
Mar. 21, 1998	0859	0.52
Mar. 21, 1998	0903	0.69
Mar. 21, 1998	0907	0.52
Mar. 21, 1998	0911	0.81
Mar. 21, 1998	0915	0.60
Mar. 21, 1998	1036-1048	0.58

1.5-nm resolution, and they likewise attributed the red-shifted wing of the line to instrument broadening. The model calculations suggest that a resolution of at least 0.6 nm is required to distinguish a red shift caused by backscattered hydrogen from the line broadening due to the instrument function. Our high-resolution auroral observations show a line profile with a broader red wing than can be explained by the instrument resolution.

From the fitting procedure we obtain values for the half width of the red wing of 0.5 to 0.7 nm, compared to the half width of the red wing of the calibration lamp of $\sim$ 0.2 nm. Table 1 summarizes the half widths of the red wing of the fitted line profiles λ_r for the data shown in Figures 4 – 6. Similar values are obtained from fits to observations from other nights.

This can also be seen from averaged spectra directly. Figure 7 shows a line profile obtained from averaging 30 auroral spectra around 0912 UT. Superimposed as a dashed line is the spectrum that we obtain from the hydrogen and xenon calibration lamps at the beginning and end of that night. When we observe the lamp spectrum, we close the window to the sky and replace it with an illuminated screen. The integration times, scan rates, and any other instrument setup are not changed. The darker environment causes the background level to drop from $\sim$ 15 to 8 counts, and the peak brightness of the lamp illuminating the screen is brighter than typical sky observations. For the comparison we have normalized both spectra to the same background level and the same peak brightness of the H_β line.

The red wing of the line profile of the lamp is entirely due to instrument resolution. If the aurora had no upward moving hydrogen, the red wing of the line profile could not extend past this lamp line profile. The red-shifted wing of the auroral line profile clearly extends to higher wavelengths than the line of the lamp. This demonstrates that the red-shifted wing is not a re-

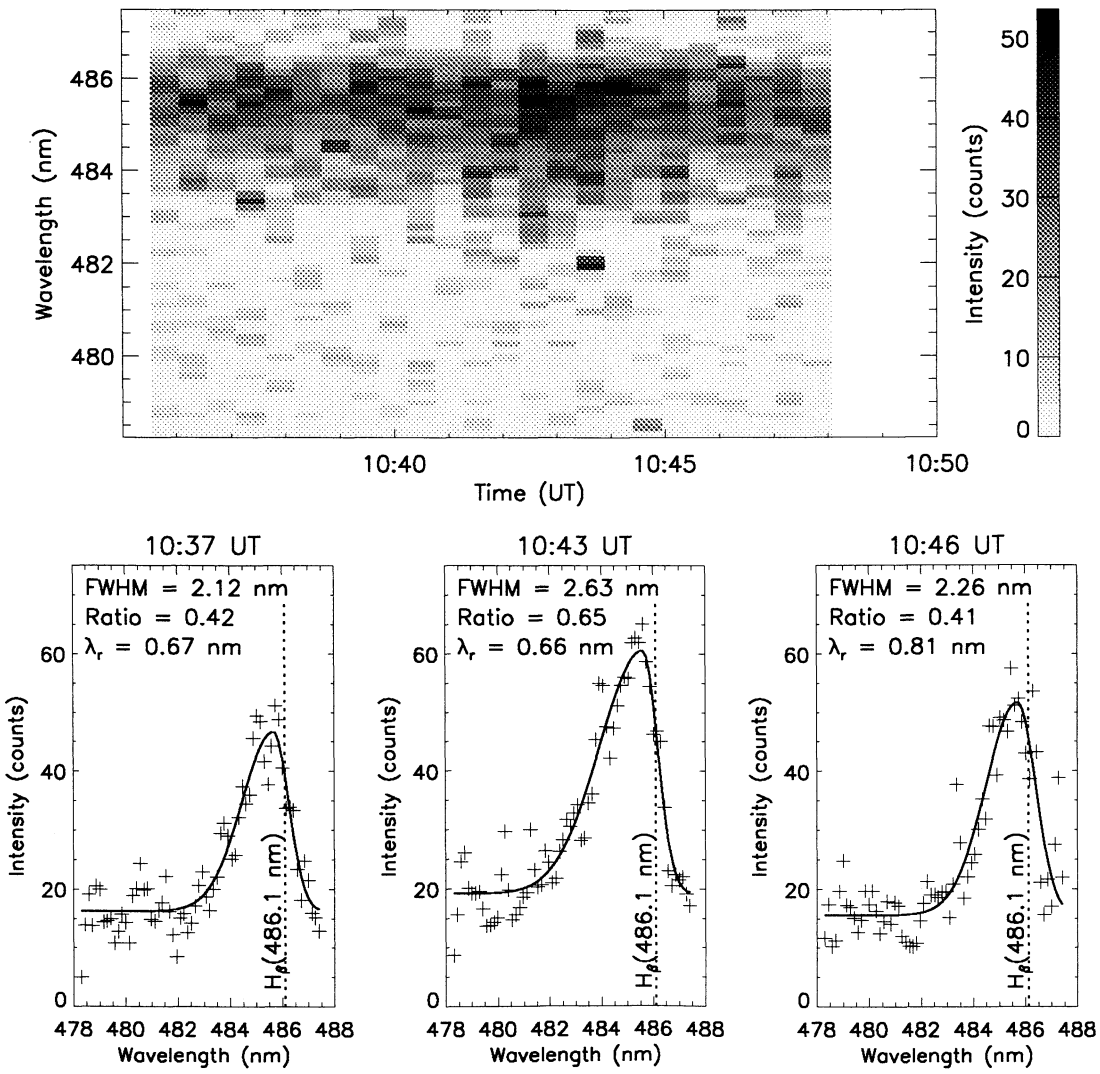

Figure 6. Same format as Figure 5. These data are from the brightest period of the night, and only two scans were averaged, giving a time resolution of 32 s.

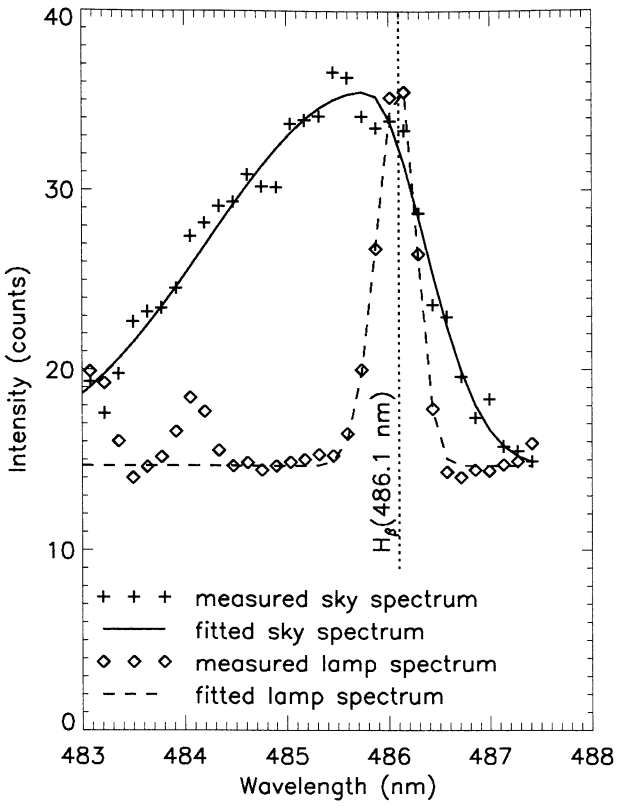

Figure 7. Observed and fitted line profiles from the aurora and from calibration lamps. The H_β line shape of the lamp spectrum shows the instrument spectral resolution. The increased brightness in the lamp spectrum at 483 and 484.3 nm results from the lines from the Xe lamp. The red wing of the auroral spectrum extends well past the unshifted H_β wavelength and past the red wing of the lamp's profile. This is a clear indication that the red wing of the auroral line profile is due to upward moving hydrogen.

sult of the instrument function but has its cause in the aurora. Since the red wing extends well above the unshifted wavelength, upward moving protons and hydrogen atoms must be present in the aurora. Comparing the red wings of the profiles in Figures 7 and 2 confirms the model predictions of red-shifted emissions due to the effects from collisional angular redistribution.

4. Summary and Conclusions

The proton-hydrogen transport models of *Galand et al.* [1998] and *Gerard et al.* [2000] predict that collisional angular redistribution of the proton-hydrogen flux causes a fraction of the precipitation to be backscattered. This manifests itself in a broadened red wing of the line profile from the red-shifted emissions originating from the upward going hydrogen. Upward moving hydrogen from mirroring protons in the converging magnetic field, or due to geometric effects from the varying slant angle of the magnetic field with latitude, cannot account for a significant contribution to the red-shifted wing of the line profile [*Eather*, 1966; *Galand and Richmond*, 1999]. In an effort to obtain experimental verification of this prediction we have deployed an Ebert-Fastie spectrometer at Poker Flat to obtain the Doppler shifted line profile of the H_β line in proton aurora. Comparing observations of the H_β line proton aurora and from a hydrogen lamp under identical conditions clearly shows a much broader red wing of the line profile in aurora. Fitting synthetic line profiles to observed spectra confirms this finding.

The proton aurora model predicts that the blue-shifted peak of the line profile shows only small variations as the mean energy of an assumed Maxwellian proton population precipitates into the thermosphere. The model calculations suggest that the increased brightness of the extreme part of the blue wing of the line profile is a more sensitive indicator for the energy of the precipitation. Since we have no independent measurements of the particle spectrum of the precipitation, we cannot directly confirm this prediction. However, during changing auroral brightness and from one auroral event to another, we found only small variations in the wavelength of the blue-shifted peak of the H_β line toward larger Doppler shift. We only show data from one night in this paper, but we found this confirmed for auroral observations over several months. Observations from Poker Flat are necessarily in the midnight sector of the auroral oval, and *Deehr et al.* [1998] find that dayside proton precipitation of near mono-energetic protons shows a more pronounced variation of the peak wavelength.

Fitting synthetic spectra to the observed line profiles, we find that the half width of the line does show more variability. From our observed and fitted spectra we can also simulate what two simpler instruments with interference filters to measure the peak brightness and the brightness at a fixed wavelength in the blue wing would observe. We selected a wavelength of 484 nm and show that the ratio of the brightness at this wavelength to the peak brightness is indeed variable. From spectra at various times during a night, all with fairly bright H_β emissions and thus high signal-to-noise ratios, we found a variation of a factor of 3 in this brightness ratio. In accordance with model predictions we thus suggest that this ratio is a good indicator of the mean energy of the precipitating protons. New instrument developments for proton aurora observations might want to take advantage of this behavior of the H_β line profile.

Acknowledgments. This research was supported at the University of Alaska by internal funds from the Geophysical Institute and by NCAR through the Advanced Study Program and the High Altitude Observatory and by NOAA through the National Research Council and the Space Environment Center.

Janet G. Luhmann thanks Jean-Claude Gerard and one other referee for their assistance in evaluating this paper.

References

Basu, B., J. R. Jasperse, R. M. Robinson, R. R. Vondrak, and D. S. Evans, Linear transport theory of auroral proton precipitation: A comparison with observations, *J. Geophys. Res., 92*, 5920, 1987.

Basu, B., J. R. Jasperse, D. J. Strickland, and R. E. Daniell Jr., Transport-theoretic model for the electron-proton-hydrogen atom aurora, 1, Theory, *J. Geophys. Res., 98*, 21,517, 1993.

Decker, D. T., B. V. Kozelov, B. Basu, J. R. Jasperse, and V. E. Ivanov, Collisional degradation of the proton-H atom fluxes in the atmosphere: A comparison of theoretical techniques, *J. Geophys. Res., 101*, 26,947, 1996.

Deehr, C. S., D. A. Lorentzen, F. Sigernes, and R. W. Smith, Dayside auroral hydrogen emission as an aeronomic signature of magnetospheric boundary layer processes, *Geophys. Res. Lett., 25*, 2111, 1998.

Dick, K. A., G. G. Sivjee, and H. M. Crosswhite, Aircraft airglow intensity measurements: Variation in OH and OI(5577), *Planet. Space Sci., 18*, 887, 1970.

Eather, R. H., Red shift of auroral hydrogen profiles, *J. Geophys. Res., 71*, 5027, 1966.

Fastie, W. G., Image forming properties of the Ebert monochomator, *J. Opt. Soc. Am., 42*, 647, 1952.

Galand, M., and A. D. Richmond, Magnetic mirroring in an incident proton beam, *J. Geophys. Res., 104*, 4447, 1999.

Galand, M., J. Lilensten, W. Kofman, and R. B. Sidje, Proton transport model in the ionosphere, 1, Multistream approach of the transport equations, *J. Geophys. Res., 102*, 22,261, 1997.

Galand, M., J. Lilensten, W. Kofman, and D. Lummerzheim, Proton transport model in the ionosphere, 2, Influence of magnetic mirroring and collisions on the angular redistribution in a proton beam, *Ann. Geophys., 16*, 1308, 1998.

Gerard, J.-C., B. Hubert, D. V. Bisikalo, and V. I. Shematovich, A model of the Lyman-α line profile in the proton aurora, *J. Geophys. Res., 105*, 15,795, 2000.

Hardy, D. A., M. S. Gussenhoven, and D. Brautigam, A statistical model of auroral ion precipitation, *J. Geophys. Res., 94*, 370, 1989.

Hedin, A. E., Extension of the MSIS thermosphere model into the middle and lower atmosphere, *J. Geophys. Res., 96*, 1159, 1991.

Jasperse, J. R., and B. Basu, Transport theoretic solutions for auroral proton and H atom fluxes and related quantities, *J. Geophys. Res., 87*, 811, 1982.

Kozelov, B. V., Influence of the dipolar magnetic field on transport of proton-H atom fluxes in the atmosphere, *Ann. Geophys., 11*, 697, 1993.

Lorentzen, D. A., F. Sigernes, and C. S. Deehr, Modeling and observations of dayside auroral hydrogen emission Doppler profiles, *J. Geophys. Res., 103*, 17,479, 1998.

Press, W. H., B. P. Flannery, S. A. Teukolsky, and W. T. Vetterling, *Numerical Recipes*, 702 pp., Cambridge Univ. Press, New York, 1989.

Sigernes F., Estimation of initial auroral proton energy fluxes from Doppler profiles, *J. Atmos. Terr. Phys., 58*, 1871, 1996.

Sigernes, F., T. Svenøe, D. A. Lorentzen, and L. T. W. Sigernes, An upgrade of the auroral Ebert-Fastie spectrometer, in *Optical Studies of Proton Aurora*, Ph.D. thesis, Paper IX, Univ. of Tromsø, Tromsø, Norway, 1996.

Søraas, F., H. R. Lindalen, K. Måseide, A. Egeland, T. A. Sten, and D. S. Evans, Proton precipitation and the H_β emission in a post-breakup auroral glow, *J. Geophys. Res., 79*, 1851, 1974.

Strickland, D. J., R. E. Daniell Jr., J. R. Jasperse, and B. Basu, Transport-theoretic model for the electron-proton-hydrogen atom aurora, 2, model results, *J. Geophys. Res., 98*, 21,533, 1993.

Synnes, S. A., F. Søraas, and J. P. Hansen, Monte-Carlo simulation of proton aurora, *J. Atmos. Sol.-Terr. Phys., 60*, 1695, 1998.

M. Galand, Center for Space Physics, Boston University, Boston, MA 02215

D. Lummerzheim, University of Alaska, Geophysical Institute, Fairbanks, AK 99775-7320. (lumm@gi.alaska.edu)

(Received February 25, 2000; revised June 8, 2000; accepted June 9, 2000.)